

Helical Majorana modes in iron based Dirac superconductors

Elio J. König¹ and Piers Coleman^{1,2}

¹*Department of Physics and Astronomy, Center for Materials Theory, Rutgers University, Piscataway, NJ 08854 USA*

²*Department of Physics, Royal Holloway, University of London, Egham, Surrey TW20 0EX, UK*

(Dated: January 14, 2019)

We propose that propagating one-dimensional Majorana fermions will develop in the vortex cores of certain iron-based superconductors in the flux phase, most notably $\text{Li}(\text{Fe}_{1-x}\text{Co}_x)\text{As}$. A key ingredient of our proposal is the presence of bulk 3D Dirac semimetallic touching points, recently observed in ARPES experiments [P. Zhang et al., *Nat. Phys.* **15**, 41 (2019)]. Using an effective $\mathbf{k} \cdot \mathbf{p}$ model which describes this class of material in the vicinity of the $\Gamma - Z$ line, we solve the Bogoliubov-deGennes Hamiltonian in the presence of a vortex, demonstrating the development of gapless one-dimensional helical Majorana modes, protected by C_4 symmetry. To expose the topological origin of these modes, we use semiclassical methods to evaluate a topological index for arbitrary dispersion beyond the $\mathbf{k} \cdot \mathbf{p}$ approximation. This allows us to relate the helical Majorana modes in a vortex line to the presence of monopoles in the Berry curvature of the normal state. We highlight various experimental signatures of our theory and discuss its possible relevance for quantum information applications and the solid state emulation of the early universe.

Can iron-based superconductors (FeSC) sustain exotic, fractionalized excitations? Recent experimental [1–6] and theoretical [7, 8] advances suggest an affirmative answer. Exploiting this, we here propose the previously unnoticed emergence of dispersive, helical Majorana states in the flux phase of certain FeSCs.

Twelve years ago, two major, independent discoveries revolutionized condensed matter physics: the observation of high temperature superconductivity in the iron-pnictides [9, 10] and the discovery of topological insulators (TIs) [11]. Iron based superconductivity has since attracted immense interest, offering a major challenge to our understanding of strongly correlated electron materials and the possibility of practical applications. This led to the discovery of a broad family of superconducting iron-based compounds. Typically, these are layered pnictides or chalcogenides where Fe^{2+} ions are enclosed in tetrahedral cages of ligand atoms. As a consequence of the associated crystal field splitting, the electronic kinetics at the Fermi energy involves the three t_{2g} orbitals of the d-shell propagating within the iron planes. Early magneto-oscillation and photoemission experiments corroborated this picture of cylindrical Fermi surfaces [12, 13].

The discovery of band topology took place in parallel with these developments [14, 15], leading to the prediction of edge, boundary, and surface states in TIs and fully gapped superconductors. Topological field theories and concepts from differential geometry suddenly found potential applications to nano-electronics and certain proposals for quantum computation devices. These concepts have been further generalized to topologically or symmetry protected Weyl and Dirac semimetals [16]. Remarkably, the excitations in those materials emulate certain aspects of elementary particle physics in solid state experiments while at the same time, the protected touching points are of potential interest for quantum sensing ap-

plications over a wide range of frequencies down to the infrared.

Until recently, the research efforts on FeSCs and topological states of matters have been largely disconnected. Spin-orbit coupling (SOC), which is a central element of most standard TIs and semimetals, was believed to be unimportant for FeSC. The discovery of SOC in photoemission spectra [17] subsequently challenged this assumption, leading to the proposal [7, 17] that for sufficiently small interlayer separations [1] an enhanced c-axis dispersion of the p_z orbitals leads to a band-crossing, driving the corresponding FeSC into a topological metal. As we shall explain in detail below, the band crossing implies that the corresponding FeSCs are topological and can sustain Majorana zero modes at the location where a magnetic flux line intersects the system's surface, Fig. 1 (c). In this work we demonstrate that this topological framework [1, 7, 8] also implies, under the right conditions, the development of dispersive, helical Majorana fermions, Fig. 1 (e) along the cores of superconducting vortices. The observation of the latter would on the one hand provide further evidence for the correctness of the proposed topological scenario and on the other hand represent the first experimental observation of these exotic excitations.

Helical Majorana fermions in one dimension correspond to a pair of gapless counter-propagating fermionic excitations which, to date, have not been experimentally observed, see Tab. I. Generically, such modes can be trapped either inside a line defect of a three dimensional material, or at the interface between two two-dimensional topological phases. The first material-specific proposal concerning the o -vortex in the B-phase of superfluid ^3He [18] was never observed, possibly because the energetics of ^3He -B favors less symmetric v -vortices [19, 20], which do not support helical Majorana modes. While additional candidate systems were proposed in subsequent

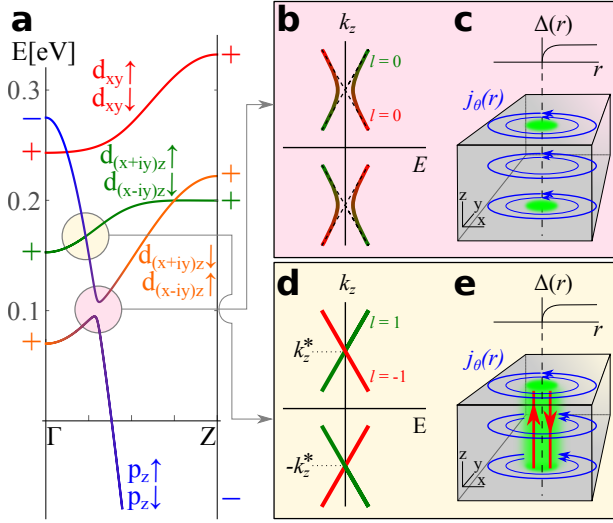


FIG. 1. Topology of iron based superconductors. (a) Band structure in the normal state. For sufficiently small lattice spacing in (001) direction, the strongly dispersive, negative parity p_z orbitals of the ligands cross the d-states along the Γ -Z line with two major consequences: First, when the chemical potential is near the SOC induced topological hybridization gap (marked by a pink disk around 0.1 eV) the many body ground state is a topological superconductor. (b) Inside a vortex core, this implies that the dispersion of bulk Caroli-Matricon-deGennes states is gapped while (c) Majorana zero modes (green pancakes) exist on the surface termination of vortex lines. Second, if the Fermi energy is close to the rotation symmetry protected Dirac node (marked by a yellow disk around 0.17 eV), (d) C_4 symmetry protects helical bulk Majorana states in the flux phase of the superconductor. (e) These are delocalized along the vortex tube.

years, gapless dispersive fermionic vortex core states have not, to our knowledge been observed. However, recent experimental advances provide evidence for chiral (i.e. unidirectional) Majorana modes at the boundaries of 2D systems, in particular a superconductor-quantum anomalous Hall heterostructure [21], a 5/2 fractional quantum Hall state [22] and at the boundary of the layered Kitaev material α -RuCl₃ [23].

Majorana modes in FeSC. Here we summarize the main physics leading to the appearance of helical Majorana subgap states in the flux phase of FeSC, when the magnetic field is aligned in (c) direction. Mathematical details are contained in [33], while the experimentally realistic case of misaligned magnetic field and crystal axis is discussed below. We shall concentrate on a case where the vortex core size, (determined by the coherence length), is much larger than the lattice spacing, so that vortex-induced inter-pocket scattering can be neglected. This permits us to concentrate on the region of the Brillouin zone which harbors the topological physics, in this case the Γ -Z line.

Along this line, the relevant electronic states may be classified by the z -component of their total angu-

lar momentum $J_z = L_z + S_z$. We may exploit the fact that the effective $\mathbf{k} \cdot \mathbf{p}$ Hamiltonian close to the Γ -Z line [1, 8, 33] features an emergent continuous rotation symmetry. Three pairs of states are important, $|d_{(x+iy)z} \downarrow\rangle, |d_{(x-iy)z} \uparrow\rangle$ (with $j_z = \pm 1/2$), $|p_z, \uparrow\rangle, |p_z, \downarrow\rangle$ (also $j_z = \pm 1/2$) and $|d_{(x+iy)z} \uparrow\rangle, |d_{(x-iy)z} \downarrow\rangle$ ($j_z = \pm 3/2$). Their dispersion is shown in Fig. 1 along with the d_{xy} bands, we used the $\mathbf{k} \cdot \mathbf{p}$ model of Ref. [8].

We first recapitulate the appearance of localized Majorana zero modes. Since j_z is the same, p_z states can hybridize with $|d_{(x+iy)z} \downarrow\rangle, |d_{(x-iy)z} \uparrow\rangle$ at intermediate k_z , leading to an avoided crossing of the bands [pink circle at 0.1 eV in Fig. 1 a)]. Since the p and d orbitals carry opposite parity, the band-crossing leads to a parity inversion at the the Z-point. The system is therefore topological [34], in the sense that, if the Fermi energy, shifted into the gap at 0.1 eV, did not cross any other bands, the system would be a 3D TI. Once the system is cooled below T_c , it is then expected [32] to host topological surface superconductivity and to develop localized Majorana zero modes at the termination of a vortex line, Fig. 1 c). The localized surface Majorana zero modes can be alternatively interpreted as the topological end states of a fully gapped, 1D superconductor inside the vortex core [8]. In the bulk, where k_z is a good quantum number the vortex hosts fermionic subgap states for each k_z near the normal state Fermi surface, Fig. 1 b). In particular, in the absence of SOC, two gapless helical bulk Majorana branches develop; since they carry angular momentum $l = 0$, a topological hybridization gap opens upon inclusion of SOC.

However, bulk FeSCs may also harbor dispersive 1D helical Majorana modes. To see this, we concentrate on the situation where the chemical potential is located near the crossing highlighted by a yellow circle at about 0.17 eV in Fig. 1 a). At this energy, semimetallic Dirac states are observed in ARPES [1]: these occur because the different j_z quantum numbers of $|p_z, \uparrow\rangle, |p_z, \downarrow\rangle$ and $|d_{(x+iy)z} \uparrow\rangle, |d_{(x-iy)z} \downarrow\rangle$ prevent a hybridization on the high symmetry line leading to a Hamiltonian of the (tilted) Dirac form $H(\mathbf{k}) = H_+(\mathbf{k}) \oplus H_-(\mathbf{k})$ [1, 33],

$$H_{\pm}(\mathbf{k}) = \begin{pmatrix} M_p(k_z) & \pm v k_x + i v k_y \\ \pm v k_x - i v k_y & M_d(k_z) \end{pmatrix}, \quad (1)$$

where $H_+(\mathbf{k})$ ($H_-(\mathbf{k})$) acts in the subspace of positive (negative) helicity spanned by $|p_z, \uparrow\rangle, |d_{(x+iy)z} \uparrow\rangle$ ($|p_z, \downarrow\rangle, |d_{(x-iy)z} \downarrow\rangle$). The dispersion $M_p(k_z), M_d(k_z)$ of the relevant p and d orbitals is plotted in Fig. 1 a) and v is the transverse velocity.

We now assume that below T_c , a spin-singlet, s-wave superconducting phase with significant intraorbital pairing, develops. In an Abrikosov lattice of vortex line, translational symmetry allows us to solve the problem at each k_z separately. In particular, at the particular value of $k_z = k_z^*$, where $M_p(k_z^*) = M_d(k_z^*)$, H_+ and H_-

	boundary of 2D systems		vortex in 3D system	
chiral	Exp.	QAH-SC [21], α -RuCl ₃ [23], $\nu = 5/2$ QH [22]	Exp.	N/A
	Th.	$p + ip$ SC [24] (Sr ₂ RuO ₄ [25]?) [Class D SC [14]]	Th.	TI-SC heterostructure [26][Weyl SSM]
helical	Exp.	N/A	Exp.	N/A
	Th.	2D NCS SC [27, 28] [class DIII SC [14, 29, 30]]	Th.	³ He-B [18], LiFe _{1-x} Co _x As (this work) [Dirac SSM]

TABLE I. Phases of matter which sustain 1+1D helical or chiral Majorana fermions. We present all experimental evidence, the first material specific theoretical proposal and generic classes of systems (in square brackets). We omitted Majorana modes which occur at fine-tuned critical points, e.g. at topological phase transitions [8, 31] or at S-TI-S junctions with flux π [32]. Abbreviations: “Exp.” = “Experiment”, “NCS” = “non-centrosymmetric”, “QAH” = “Quantum anomalous Hall”, “QH” = “Quantum Hall”, “SC” = “superconductor”, “SSM” = “superconducting semimetal”, “Th.” = “Theory”.

separately take the form of a TI surface state. Consequently [32], for each helicity a non-degenerate Majorana zero mode appears in each vortex. Now in contrast to the case of Fig. 1 b), left and right moving modes carry different angular momenta $l = \pm 1$ so that they can not be mixed by any perturbation which respects the C_4 symmetry (in particular not by a Zeeman field). This leads to the linear helical dispersion near k_z^* .

Solution of Bogoliubov-deGennes Hamiltonian. To confirm these heuristic arguments, we have perturbatively solved [33] the Bogoliubov-deGennes Hamiltonian of a topological FeSC with a single vortex. Here, we concentrate on states near k_z^* , so that $\mathcal{H} = \bigoplus_{\pm} \mathcal{H}_{\pm}$ with $\mathcal{H}_{\pm} = (H_{\pm} - \mu)\tau_z + \Delta(\mathbf{r})(\tau_x + i\tau_y)/2 + \Delta^*(\mathbf{r})(\tau_x - i\tau_y)/2$. The Fermi energy μ is measured from the Dirac point, $\Delta(\mathbf{r}) = |\Delta(r)|e^{i\theta}$ is the superconducting gap ($|\Delta(\infty)| \equiv \Delta$) and $\tau_{x,y,z}$ are Pauli matrices in Nambu space. Assuming isotropic vortices, we expanded the wave function in angular momenta and k_z , $\Psi_{\pm}(\mathbf{r}) = \sum_{l,k_z} e^{ik_z z} U_{\pm}^{(l)}(\theta) \Psi_{\pm}^{(l)}(r, k_z)$, with $U_{+}^{(l)} = \text{diag}(u_{(l)}, u_{(l-1)})$, $U_{-}^{(l)} = \text{diag}(u_{(-l-1)}^*, u_{(-l)}^*)$ and $u_{(l)} = (e^{il\theta - i\pi/4}, e^{i(l-1)\theta + i\pi/4})$. At $l = 1$ ($l = -1$) a chiral symmetry in the l -th sector $\mathcal{H}_{+}^{(l)}$ ($\mathcal{H}_{-}^{(l)}$) allows to explicitly construct unpaired zero energy solutions $\Psi_{\pm}^{(l=\pm 1)}(r, k_z^*) = (v_{\pm}(r), \pm v_{\mp}(r))$, where $v_{\pm}(r) = \mathcal{N}e^{-\int_0^r \Delta(r')dr'} (\mp J_{1/2 \pm 1/2}(\mu r/v), J_{1/2 \mp 1/2}(\mu r/v))$, \mathcal{N} is a normalization constant and $J_{\nu}(x)$ are Bessel functions. We use these solutions to perturbatively include momenta $p_z = k_z - k_z^*$, a Zeeman field E_Z and unequal $\Delta_p - \Delta_d = \delta\Delta \neq 0$. By projecting onto the low-energy space we obtain the effective Hamiltonian

$$\mathcal{H}_{\text{eff}} = \bigoplus_{\pm} \mp [v_M(\mu/\Delta)p_z + w_M(\mu/\Delta)\delta\Delta - E_Z], \quad (2)$$

which demonstrates the appearance of helical Majorana modes. In the limit $\mu \gg \Delta$ we obtain $v_M \sim \Delta^2 \partial_{k_z^*} [M_p(k_z^*) - M_d(k_z^*)]/\mu^2$ and $w_M \sim \Delta/\mu$. The velocity of helical Majorana modes in vortices of ³He - B has an analogous parametrical dependence [18].

Topological origin of helical Majorana modes. The crystalline topological protection of the helical Majorana modes in the flux phase of FeSC can be under-

stood as follows. First, we note that in the normal state, crystalline symmetries, in particular C_4 , impose the decoupling of Hamiltonian (1) into the direct sum of two decoupled helical sectors. Within H_+ (H_-), two Weyl points of opposite topological charge ± 1 (∓ 1) appear at $(0, 0, \pm k_z^*)$, Fig. 2 a). Since crystalline symmetry ensures perfect decoupling, it is favorable to concentrate on a given sector in these explanations and superimpose both sectors in the end. The Berry flux connecting the two Weyl points implies a quantum anomalous Hall state for $k_z \in (-k_z^*, k_z^*)$ [35]. The resulting family of chiral edge states forms a Fermi arc in the surface Brillouin of the system, see Fig. 2 b). In view of their chiral nature, Fermi arc states can only terminate at a k_z which sustains bulk states - i.e. at the projection of the Weyl points. The presence of these critical bulk states is ensured since the system undergoes a topological phase transition as a function of k_z .

We now turn to the superconducting case in the flux phase, for which a vortex core represents a normal state cylinder inside of a fully gapped superconducting background. At each $k_z \in (-k_z^*, k_z^*)$ the boundary of the vortex core resembles an interface between quantum anomalous Hall state and a topological superconductor. This leads to a chiral Majorana encircling the cylinder - this is the Majorana analog [1] of Fermi arc states (purple circles Fig. 2). At the same time, for $k_z \notin [-k_z^*, k_z^*]$ Fermi arc states are absent. As explained above, edge states may only disappear as a function of k_z when the bulk is critical, therefore it follows that topologically protected vortex core subgap states must cross the Fermi energy at $\pm k_z^*$.

We conclude this discussion with two remarks. (1) For typical vortex core diameters ξ the chiral Majorana edge states are gapped by finite size effects, yet the above topological argument is still valid. In particular, as in the case of a 3D TI surface, the magnetic flux prevents the critical bulk (= vortex core) states at $\pm k_z^*$ from gapping. (2) Taking into account that H_+ and H_- sectors have opposite helicity, the actual state for $k_z \in (-k_z^*, k_z^*)$ is a quantum spin Hall insulator, and Fermi arc states are helical rather than chiral.

Index theorem. To support the qualitative arguments

introduced above, we now demonstrate that the crystalline topological protection of the helical Majorana modes is encoded in the following index of a generic Bogoliubov-deGennes-Hamiltonian $\mathcal{H} = \mathcal{H}_+ \oplus \mathcal{H}_-$ with two helical sectors [36]

$$\begin{aligned} N(k_z) &= \int \frac{d\epsilon}{2\pi} \text{ReTr} \left\{ \sum_{\pm} (\mp 1) [i\epsilon - \mathcal{H}_{\pm}(k_z)]^{-1} \right\} \\ &= \frac{1}{2} \sum_n \text{sign}(E_{n,+}(k_z)) - \frac{1}{2} \sum_n \text{sign}(E_{n,-}(k_z)). \end{aligned} \quad (3)$$

Here, translational symmetry along the vortex line permits us to consider $\mathcal{H}_{\pm}(k_z)$ for each k_z , separately. Since for all eigenstates apart of the anomalous helical Majorana branch $E_{n,+}(k_z) = E_{n,-}(k_z)$, the difference of two divergent sums acquires a natural regularization scheme. On these grounds a jump in the sign of $N(k_z)$ signals the node of a helical Majorana mode.

We semiclassically evaluate Eq. (3) for a generic Hamiltonian under the assumption that the Fermi surface in each helical sector is non-degenerate and the vortex of winding ν_v is isotropic. In the semiclassical limit $k_F \xi \gg 1$, where ξ is the vortex radius (coherence length) and k_F the Fermi momentum of the 2D problem at given k_z , only the first derivative of Δ enters. The index may then be expressed [33] as an integral over phase space coordinates

$$N(k_z) = \nu_v \int \frac{d^2 P}{2\pi} [\Omega_z^+ - \Omega_z^-] \int_0^\infty d\mathbf{R} \cdot \vec{\nabla}_X n(\mathbf{R}, \mathbf{P}). \quad (4)$$

Here, the component of the normal state Berry curvature along the vortex line $\Omega_z^\pm = \Omega_z^\pm(P_x, P_y, P_z)$ of each sector should be evaluated at given $P_z = k_z$. The same is true for the semiclassical quasiparticle occupation $n(\mathbf{R}, \mathbf{P}) = 1/2 - [\epsilon(\mathbf{P}, k_z) - \mu]/2\sqrt{[\epsilon(\mathbf{P}, k_z) - \mu]^2 + |\Delta(\mathbf{R}, \mathbf{P}, k_z)|^2}$, where $\epsilon(\mathbf{P}, P_z) = \epsilon(P_x, P_y, P_z)$ is the normal state dispersion. In each helical sector, Eq. (4) measures the difference between the (quantum) anomalous Hall response carried by superconducting quasiparticles at $R = \infty$ and inside normal vortex core $R = 0$. Near a Dirac node, $\Omega_z^+ = -\Omega_z^-$ has a sign change as a function of k_z , and thus Eq. (4) implies the emergence of helical Majorana states.

In contrast with earlier index theorems and topological invariants for gapless vortex core states [36–40], Eq. (4) relates the appearance of helical Majorana modes to the Berry curvature monopoles. However, the leading order expansion in gradients employed in Eq. (4) is unable to capture the hybridization (gapping) of subgap states for vortices with an even winding number.

Experimental realization. It is important to stress that the non-interacting topological picture which we employed relies on ab-initio density functional theory (DFT) with limited reliability in the regime of realistic substantial interactions. In order to provide support for the topological paradigm associated with Fig. 1, we briefly summarize the topological features

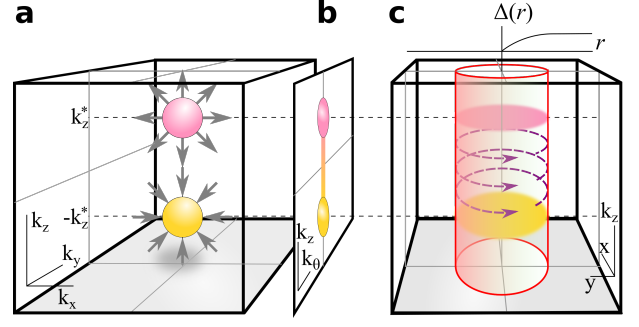


FIG. 2. (a) As the crystal momentum k_z is varied, the Dirac nodes in the normal state bulk Brillouin-zone imply a family of quantum spin Hall states for each momentum $k_z \in (-k_z^*, k_z^*)$ (here Weyl nodes in the spin down sector are shown). The topological phase transition at $k_z = \pm k_z^*$ imposes the existence of critical bulk states, which coincide with the termination points of the Fermi arc in the surface Brillouin zone (b). (c) A superconducting vortex consists of a metallic core enclosed by a fully gapped superconductor which formally leads to Majorana Fermi arc states (purple, dashed) encircling the core. While such states are typically gapped out due to the finite core diameter ξ , the change in topology at $\pm k_z^*$ enforces the spectral flow of states presented in Fig. 1 (d).

of iron-based superconductors which were observed to date. Firstly, topological Dirac surface states have been observed in $\text{Fe}(\text{Te}_x\text{Se}_{1-x})$ and $\text{Li}(\text{Fe}_{1-x}\text{Co}_x)\text{As}$ using (S)ARPES, both in the normal and superconducting states [2]. Secondly, photoemission evidence of the 3D Dirac semimetallic bulk states in the normal state was also reported in Ref. [1]. Thirdly, zero bias peaks in vortices of the flux phase of $\text{Fe}(\text{Te}_x\text{Se}_{1-x})$ [3, 5, 6] and $(\text{Li}_{1-x}\text{Fe}_x)\text{OHFeSe}$ [4] were associated with Majorana bound states of Fig. 1 c). It is important to bear in mind that other groups [41] only observed conventional Caroli-deGennes-Matricon [42] states. Finally, a robust zero bias peak, akin to a Majorana bound state was also reported to occur at excess iron atoms of FeTe [43] – this highly unexpected phenomenon can not be explained [44] within the simplest topological band theory outlined above but corroborates the topological prospects of FeSC.

From these arguments, built around the topological bandstructure of Fig. 1 a), we think that there is well-founded hope to realize helical Majorana modes in the vortex cores of FeSC Dirac semimetals. Conversely, a successful experimental observation of helical Majorana modes in FeSC could be used as further evidence that the topological paradigm proposed for FeSC on the grounds of DFT is at least qualitatively correct.

$\text{Li}(\text{Fe}_{1-x}\text{Co}_x)\text{As}$, in which 3D bulk Dirac cones were observed in (S)ARPES at a doping level of $x = 0.09$ [1], is a strong candidate for these Majorana modes. It exhibits a $T_c(x = 0.09) \approx 9\text{K}$ [45] and, like all FeSC, is a strongly type-II superconductor. To get an insight of typical experimental scales we compare to an STM

study [46] of vortices in the parent compound LiFeAs (here $T_c = 18K$ is larger but comparable). Vortices are observable at $B \geq 0.1T$ corresponding to typical vortex spacing of $l_B \lesssim 80$ nm, while the core radius is $\xi \approx 2.5$ nm. Therefore, intervortex tunneling, which would gap the zero modes is expected to be weak. Furthermore, the large ratio $\Delta/E_F \sim 0.5 \dots 1$ implies that the helical Majorana band should be well separated in energy from conventional Caroli-deGennes-Matricon states [42].

A pair of helical Majorana modes displays universal thermal conductivity of $\kappa_0 = \mathcal{L}T e^2/h$ with $\mathcal{L} = \pi^2 k_B^2/3e^2$ being the Lorenz number [47], and the observation of this linear thermal conductivity provides a key way to test our theory. In the flux phase, each of the Φ/Φ_0 vortices hosts 2 pairs of Majoranas, so that the linear magnetic field dependence $\kappa_{\text{tot}} = 2\kappa_0\Phi/\Phi_0$ of the total heat transport along the magnetic field direction can be easily discriminated from the phonon background. A similar effect occurs in the specific heat $C = 2c_0\Phi/\Phi_0$ with $c_0 = \pi k_B^2 T/3v_M$. Furthermore, STM measurements are expected to signal a spatially localized signal in the center of the vortex, with nearly constant energy dependence of the tunneling density of states $\nu(E) \xrightarrow{E \rightarrow 0} 1/\pi v_M$.

Summary and Outlook. In conclusion, we have demonstrated that gapless, dispersing Majorana modes are expected to develop in the vortex cores, in the flux phase of iron-based superconductors, see Fig. 1 e). These states are protected by crystalline C_4 symmetry, but generic topological considerations, Fig. 2 and Eq. (4), indicate a substantial robustness to weak misalignments. The hallmark signature is the extensive dependence of various thermodynamic and transport observables on the number of vortices, i.e. on the external magnetic field.

The proposed setup would lead to the first experimental realization of helical 1+1D Majorana fermions. We note that analogous excitations at the edges of topological superconductors have been proposed as a way to implement [48, 49] braiding operations for topological quantum computing. Another interesting observation is that superconducting and superfluid vortices are condensed matter analogs of cosmic strings, line defects envisaged to develop in the early universe in response to spontaneous symmetry breaking in a (grand) unified field theory. Defects capable of trapping dispersive fermionic zero modes [50] may occur in speculative SO(10) GUTs but also in standard electroweak theory [51, 52] and in either case the interaction of cosmic strings with magnetic fields leads to a sizeable baryogenesis. Helical Majorana modes in the vortex of FeSC may permit an experimental platform for testing these ideas.

NOTE ADDED

In the last stage of preparing the manuscript, a preprint appeared [53] which discusses 1+1D Majorana

modes in the vortex of a weak TI phase of certain FeSC. The authors of Ref. [53] also report to address gapless Majorana modes in vortices of FeSC Dirac semimetals in an unpublished reference.

ACKNOWLEDGEMENTS

We acknowledge useful discussions with P.Y. Chang, H. Ding, V. Drouin-Touchette, Y. Komijani, P. Kotetes, M. Scheurer, P. Volkov. This material is based upon work supported by the U.S. Department of Energy, Office of Science, Office of Basic Energy Sciences, under Award DE-FG02-99ER45790 (Elio Koenig and Piers Coleman). This research is funded in part by a QuantEmX grant from ICAM and the Gordon and Betty Moore Foundation through Grant GBMF5305.

-
- [1] P. Zhang, Z. Wang, X. Wu, K. Yaji, Y. Ishida, Y. Kohama, G. Dai, Y. Sun, C. Bareille, K. Kuroda, T. Kondo, K. Okazaki, K. Kindo, X. Wang, C. Jin, J. Hu, R. Thomale, K. Sumida, S. Wu, K. Miyamoto, T. Okuda, H. Ding, G. D. Gu, T. Tamegai, T. Kawakami, M. Sato, and S. Shin, *Nat. Phys.* **15**, 41 (2019).
 - [2] P. Zhang, K. Yaji, T. Hashimoto, Y. Ota, T. Kondo, K. Okazaki, Z. Wang, J. Wen, G. D. Gu, H. Ding, and S. Shin, *Science* **360**, 182 (2018).
 - [3] D. Wang, L. Kong, P. Fan, H. Chen, S. Zhu, W. Liu, L. Cao, Y. Sun, S. Du, J. Schneeloch, R. Zhong, G. Gu, L. Fu, H. Ding, and H.-J. Gao, *Science* **362**, 333 (2018).
 - [4] Q. Liu, C. Chen, T. Zhang, R. Peng, Y.-J. Yan, C.-H.-P. Wen, X. Lou, Y.-L. Huang, J.-P. Tian, X.-L. Dong, G.-W. Wang, W.-C. Bao, Q.-H. Wang, Z.-P. Yin, Z.-X. Zhao, and D.-L. Feng, *Phys. Rev. X* **8**, 041056 (2018).
 - [5] T. Machida, Y. Sun, S. Pyon, S. Takeda, Y. Kohsaka, T. Hanaguri, T. Sasagawa, and T. Tamegai, arXiv preprint arXiv:1812.08995 (2018).
 - [6] L. Kong, S. Zhu, M. Papaj, L. Cao, H. Isobe, W. Liu, D. Wang, P. Fan, H. Chen, Y. Sun, S. Du, J. Schneeloch, R. Zhong, G. Gu, L. Fu, H.-J. Gao, and H. Ding, arXiv preprint arXiv:1901.02293 (2019).
 - [7] Z. Wang, P. Zhang, G. Xu, L. K. Zeng, H. Miao, X. Xu, T. Qian, H. Weng, P. Richard, A. V. Fedorov, H. Ding, X. Dai, and Z. Fang, *Phys. Rev. B* **92**, 115119 (2015).
 - [8] G. Xu, B. Lian, P. Tang, X.-L. Qi, and S.-C. Zhang, *Phys. Rev. Lett.* **117**, 047001 (2016).
 - [9] Y. Kamihara, H. Hiramatsu, M. Hirano, R. Kawamura, H. Yanagi, T. Kamiya, and H. Hosono, *J. Am. Chem. Soc.* **128**, 10012 (2006).
 - [10] H. Takahashi, K. Igawa, K. Arii, Y. Kamihara, M. Hirano, and H. Hosono, *Nature* **453**, 376 (2008).
 - [11] M. König, S. Wiedmann, C. Brüne, A. Roth, H. Buhmann, L. W. Molenkamp, X.-L. Qi, and S.-C. Zhang, *Science* **318**, 766 (2007).
 - [12] D. H. Lu, M. Yi, S. K. Mo, A. S. Erickson, J. Analytis, J. H. Chu, D. J. Singh, Z. Hussain, T. H. Geballe, I. R. Fisher, and Z. X. Shen, *Nature* **455**, 81 (2008).

- [13] A. I. Coldea, J. D. Fletcher, A. Carrington, J. G. Analytis, A. F. Bangura, J.-H. Chu, A. S. Erickson, I. R. Fisher, N. E. Hussey, and R. D. McDonald, *Phys. Rev. Lett.* **101**, 216402 (2008).
- [14] A. P. Schnyder, S. Ryu, A. Furusaki, and A. W. Ludwig, *Phys. Rev. B* **78**, 195125 (2008).
- [15] B. Bernevig and T. Hughes, *Topological Insulators and Topological Superconductors* (Princeton University Press, 2013).
- [16] N. P. Armitage, E. J. Mele, and A. Vishwanath, *Rev. Mod. Phys.* **90**, 015001 (2018).
- [17] S. V. Borisenko, D. V. Evtushinsky, Z. H. Liu, I. Morozov, R. Kappenberger, S. Wurmehl, B. Büchner, A. N. Yaresko, T. K. Kim, M. Hoesch, T. Wolf, and N. D. Zhigadlo, *Nat. Phys.* **12**, 311 (2015).
- [18] T. S. Misirpashaev and G. Volovik, *Phys. B (Amsterdam, Neth.)* **210**, 338 (1995).
- [19] D. Vollhardt and P. Wölfle, *The Superfluid Phases of Helium 3*, Dover Books on Physics (Dover Publications, 2013).
- [20] G. Volovik, *The Universe in a Helium Droplet*, International Series of Monographs on Physics (Clarendon Press, 2003).
- [21] Q. L. He, L. Pan, A. L. Stern, E. C. Burks, X. Che, G. Yin, J. Wang, B. Lian, Q. Zhou, E. S. Choi, K. Murata, X. Kou, Z. Chen, T. Nie, Q. Shao, Y. Fan, S.-C. Zhang, K. Liu, J. Xia, and K. L. Wang, *Science* **357**, 294 (2017).
- [22] M. Banerjee, M. Heiblum, V. Umansky, D. E. Feldman, Y. Oreg, and A. Stern, *Nature* **559**, 205 (2018).
- [23] Y. Kasahara, T. Ohnishi, Y. Mizukami, O. Tanaka, S. Ma, K. Sugii, N. Kurita, H. Tanaka, J. Nasu, Y. Motome, *et al.*, arXiv preprint arXiv:1805.05022 (2018).
- [24] G. E. Volovik, *Sov. Phys. JETP* **67**, 1804 (1988), [ZhETF **94**, 123 (1988)].
- [25] T. M. Rice and M. Sigrist, *J. Phys.: Condens. Matter* **7**, L643 (1995).
- [26] T. Meng and L. Balents, *Phys. Rev. B* **86**, 054504 (2012).
- [27] Y. Tanaka, T. Yokoyama, A. V. Balatsky, and N. Nagaosa, *Phys. Rev. B* **79**, 060505 (2009).
- [28] M. Sato and S. Fujimoto, *Phys. Rev. B* **79**, 094504 (2009).
- [29] R. Roy, arXiv preprint arXiv:0803.2868 (2008).
- [30] X.-L. Qi, T. L. Hughes, S. Raghu, and S.-C. Zhang, *Phys. Rev. Lett.* **102**, 187001 (2009).
- [31] P. Hosur, P. Ghaemi, R. S. K. Mong, and A. Vishwanath, *Phys. Rev. Lett.* **107**, 097001 (2011).
- [32] L. Fu and C. L. Kane, *Phys. Rev. Lett.* **100**, 096407 (2008).
- [33] Supplementary materials to this publication.
- [34] L. Fu and C. L. Kane, *Phys. Rev. B* **76**, 045302 (2007).
- [35] Strictly speaking, if k_z states are filled up to a finite Fermi momentum k_F around the Weyl node, quantization occurs for the smaller interval $k_z \in (-k_z^* + k_F, k_z^* - k_F)$.
- [36] G. Volovik, *JETP Letters* **49**, 391 (1989).
- [37] E. J. Weinberg, *Phys. Rev. D* **24**, 2669 (1981).
- [38] J. C. Y. Teo and C. L. Kane, *Phys. Rev. B* **82**, 115120 (2010).
- [39] X.-L. Qi, E. Witten, and S.-C. Zhang, *Phys. Rev. B* **87**, 134519 (2013).
- [40] B. Roy and P. Goswami, *Phys. Rev. B* **89**, 144507 (2014).
- [41] M. Chen, X. Chen, H. Yang, Z. Du, X. Zhu, E. Wang, and H.-H. Wen, *Nat. Comm.* **9**, 970 (2018).
- [42] C. Caroli, P. G. De Gennes, and J. Matricon, *Phys. Lett.* **9**, 307 (1964).
- [43] J.-X. Yin, Z. Wu, J.-H. Wang, Z.-Y. Ye, J. Gong, X.-Y. Hou, L. Shan, A. Li, X.-J. Liang, X.-X. Wu, J. Li, C.-S. Ting, Z.-Q. Wang, J.-P. Hu, P.-H. Hor, H. Ding, and S. H. Pan, *Nat. Phys.* **11**, 543 (2015).
- [44] K. Jiang, X. Dai, and Z. Wang, arXiv preprint arXiv:1808.07072 (2018).
- [45] Y. M. Dai, H. Miao, L. Y. Xing, X. C. Wang, P. S. Wang, H. Xiao, T. Qian, P. Richard, X. G. Qiu, W. Yu, C. Q. Jin, Z. Wang, P. D. Johnson, C. C. Homes, and H. Ding, *Phys. Rev. X* **5**, 031035 (2015).
- [46] T. Hanaguri, K. Kitagawa, K. Matsubayashi, Y. Mazaki, Y. Uwatoko, and H. Takagi, *Phys. Rev. B* **85**, 214505 (2012).
- [47] M. J. Pacholski, C. W. J. Beenakker, and I. Adagideli, *Phys. Rev. Lett.* **121**, 037701 (2018).
- [48] H. Hu, I. I. Satija, and E. Zhao, arxiv preprint arXiv:1812.05014 (2018).
- [49] B. Lian, X.-Q. Sun, A. Vaezi, X.-L. Qi, and S.-C. Zhang, *Proc. Natl. Acad. Sci. U.S.A.* **115**, 10938 (2018).
- [50] R. Jackiw and P. Rossi, *Nucl. Phys. B* **190**, 681 (1981).
- [51] A. Vilenkin and E. Shellard, *Cosmic Strings and Other Topological Defects*, Cambridge Monographs on Mathematical Physics (Cambridge University Press, 2000).
- [52] E. Witten, *Nucl. Phys. B* **249**, 557 (1985).
- [53] S. Qin, L. Hu, X. Wu, X. Dai, C. Fang, F.-C. Zhang, and J. Hu, arXiv eprint arXiv:1901.03120 (2019).

Supplementary materials on
"Helical Majorana modes in iron based Dirac superconductors"

Elio J. König¹ and Piers Coleman^{1,2}

¹*Department of Physics and Astronomy, Center for Materials Theory, Rutgers University, Piscataway, NJ 08854*

^{1,2}*Department of Physics, Royal Holloway, University of London, Egham, Surrey TW20 0EX, UK*

The supplementary materials contain mathematical details for the results presented in the main text and contains a section on the perturbative Majorana solution and a section on the index theorem.

PERTURBATIVE MAJORANA SOLUTION

Normal state $\mathbf{k} \cdot \mathbf{p}$ Hamiltonian

We employ the $\mathbf{k} \cdot \mathbf{p}$ model as introduced in Refs. [1, 8]. It is favorable to express the Hamiltonian in the basis $(\Psi_\uparrow, \Psi_\downarrow)$ with $\Psi_\uparrow = (|z, \uparrow\rangle, |(x+iy)z, \uparrow\rangle, |(x-iy)z, \uparrow\rangle, |xy, \uparrow\rangle)$ and $\Psi_\downarrow = (|z, \downarrow\rangle, |(x-iy)z, \downarrow\rangle, |(x+iy)z, \downarrow\rangle, |xy, \downarrow\rangle)$. Note the different order of $|(x \pm iy)z\rangle$ orbitals in the spin up (\uparrow) and spin down (\downarrow) sectors. Then

$$H(\mathbf{k}) = \left(\begin{array}{cccc|cccc} M_1 & \bar{\chi}k_+ & -\bar{\chi}k_- & 0 & \mathbf{0} & \mathbf{0} & \bar{\lambda}_3 & 0 \\ \bar{\chi}k_- & M_2^+ & B^\dagger & \bar{\gamma}k_+ & \mathbf{0} & \mathbf{0} & 0 & -\bar{\lambda}_2 \\ -\bar{\chi}k_+ & B & M_2^- & \bar{\gamma}k_- & \bar{\lambda}_3 & 0 & 0 & 0 \\ 0 & \bar{\gamma}k_- & \bar{\gamma}k_+ & M_3 & 0 & \bar{\lambda}_2 & 0 & 0 \\ \hline \mathbf{0} & \mathbf{0} & \bar{\lambda}_3 & 0 & M_1 & -\bar{\chi}k_- & \bar{\chi}k_+ & 0 \\ \mathbf{0} & \mathbf{0} & 0 & \bar{\lambda}_2 & -\bar{\chi}k_+ & M_2^+ & B & \bar{\gamma}k_- \\ \bar{\lambda}_3 & 0 & 0 & 0 & \bar{\chi}k_- & B^\dagger & M_2^- & \bar{\gamma}k_+ \\ 0 & -\bar{\lambda}_2 & 0 & 0 & 0 & \bar{\gamma}k_+ & \bar{\gamma}k_- & M_3 \end{array} \right) := \left(\begin{array}{c|c} H_\uparrow & \Lambda \\ \hline \Lambda^T & H_\downarrow \end{array} \right). \quad (\text{S1})$$

Here, we used the notation $k_\pm = k_x \pm ik_y$, $\bar{\chi} = \chi/\sqrt{2}$, $\bar{\gamma} = \sin(k_z)\gamma/\sqrt{2}$, $M_2^\pm = M_2 \pm \lambda_1$, $\bar{\lambda}_2 = \lambda_2\sqrt{2}$, $\bar{\lambda}_3 = \lambda_3 \sin(k_z)\sqrt{2}$, $M_{1,2,3} = M_{1,2,3}^0 + M_{1,2,3}^1(k_x^2 + k_y^2) + M_{1,2,3}^2(1 - \cos(k_z))$, $B = \beta k_+^2$, where $\chi, \gamma, \beta, M_{1,2,3}^{1,2,3}, \lambda_{1,2,3}$ were introduced in Ref. [1] of the main text.

The advantage of this basis is twofold. First, time reversal symmetry is represented simply by $\sigma_y K$ (K being complex conjugation), since the different ordering of up-spin and down-spin takes into account the mapping of $|(x \pm iy)z\rangle \rightarrow |(x \mp iy)z\rangle$. Second, the Dirac touching point at $M_1 = M_2^+$ is apparent, see the submatrix of boldface zeros. Ultimately, this follows from $|z, \sigma\rangle$ being $j_z = \pm 1/2$ and $|(x \pm iy)z, \uparrow\rangle, |(x - iy)z, \downarrow\rangle$ being $j_z = \pm 3/2$ and therefore they cannot mix (in contrast to reversed spin components of $|(x \pm iy)z\rangle$, which lead to a topological gap induced by $\bar{\lambda}_3$.)

In the main text, we introduce a Dirac Hamiltonian in Eq. (1). We identify the parameters as $M_p \simeq M_1$, $M_d \simeq M_2^+$ and $v \simeq \bar{\chi}$ up to corrections of higher order in $\bar{\lambda}_{2,3}$. Such corrections stem from the perturbative integration of orbitals which near the Dirac touching point are off-shell.

Superconductivity

In general, the inclusion of spin-singlet superconductivity in the basis $(\Phi, i\sigma_y\Phi^*)$ (Φ being a multiorbital wave function) leads to

$$\mathcal{H} = \left(\begin{array}{cc} H - \mu & \Delta \\ \Delta^\dagger & \mu - H \end{array} \right). \quad (\text{S2})$$

Here, Δ is a matrix in orbital space but trivial in spin space. The Pauli principle imposes $\Delta = \Delta^T$, time reversal symmetry, if present, implies then $\Delta^T = \Delta^\dagger$. If furthermore s-wave pairing is assumed, the matrix function $\Delta(\mathbf{k})$ has the same symmetries as the Hamiltonian, i.e. a form analogous to Eq. (S1). For simplicity, we concentrate only on the constant part, which is perfectly diagonal $\Delta = \text{diag}(\Delta_1, \Delta_2^+, \Delta_2^-, \Delta_3)$.

In the presence of a vortex tube in the (001) direction, $\Delta \rightarrow \Delta(r)e^{i\theta}$ and time reversal symmetry is broken. We use cylindrical coordinates $(x, y, z) = (r \cos(\theta), r \sin(\theta), z)$. The particle-hole symmetry of the superconducting Hamiltonian $C\mathcal{H}^*C = -\mathcal{H}$ with $C = \sigma_y\tau_y$ persists even in the presence of the vortex. In view of rotational symmetry, it is

possible to assign the quantum numbers k_z (momentum in z -direction), l (angular momentum in $x-y$ plane) and n (radial quantum number) in the bulk of the system. Particle hole symmetry implies the appearance of pairs of eigenstates $\Psi_{k_z,n,l}(\mathbf{x})$ and $\sigma_y \tau_y \Psi_{k_z,n,l}^*(\mathbf{x}) \propto \sigma_y \tau_y \Psi_{-k_z,n,-l}(\mathbf{x})$ with opposite eigenenergy $E_{k_z,n,l} = -E_{-k_z,n,-l}$. Furthermore, there is an inversion symmetry $z \rightarrow -z, \theta \rightarrow \theta + \pi$ which is represented by $P = \text{diag}(-\mathbf{1}_\sigma, \mathbf{1}_\sigma, \mathbf{1}_\sigma, \mathbf{1}_\sigma; \mathbf{1}_\sigma, -\mathbf{1}_\sigma, -\mathbf{1}_\sigma, -\mathbf{1}_\sigma)$ and implies degeneracy of $E_{k_z,n,l}$ and $E_{-k_z,n,l}$.

Majorana solutions

We now switch to the basis $(\Psi_\uparrow, \Psi_\downarrow, \Psi_\downarrow^*, -\Psi_\uparrow^*)$, this corresponds to an additional rotation in Nambu space swapping second and third blocks. We obtain

$$\mathcal{H} = \left(\begin{array}{cc|cc} H_\uparrow - \mu & \Delta & \Lambda & 0 \\ \Delta^* & \mu - H_\uparrow & 0 & -\Lambda \\ \hline \Lambda^T & 0 & H_\downarrow - \mu & \Delta \\ 0 & -\Lambda^T & \Delta^* & \mu - H_\downarrow \end{array} \right). \quad (\text{S3})$$

The topologically most interesting features of the bulk spectrum are given by the crossing $M_1(k_z) = M_2^+(k_z)$ (Dirac point) and the anticrossing $M_1(k_z) = M_2^-(k_z)$ (topological gap). It is therefore sufficient to retain only $z, (x + iy)z$ and $(x - iy)z$ states. In this section we absorb the velocity into redefined length scales such that $\bar{\chi}k_\pm = -i(\partial_x \pm i\partial_y)$. We further set $\bar{\beta} = \beta/\bar{\chi}^2$, $\bar{M}_{1,2,3} = M_{1,2,3}^{(0)} + M_{1,2,3}^{(2)}2(1 - \cos(k_z)) - (M_{1,2,3}^{(1)}/\bar{\chi}^2)(\partial_x^2 + \partial_y^2) - \mu$, so that

$$H_\uparrow = \begin{pmatrix} \bar{M}_1 & p_+ & -p_- \\ p_- & \bar{M}_2^+ & \bar{\beta}p_-^2 \\ -p_+ & \bar{\beta}p_+^2 & \bar{M}_2^- \end{pmatrix}, \quad H_\downarrow = \begin{pmatrix} \bar{M}_1 & -p_- & p_+ \\ -p_+ & \bar{M}_2^+ & \bar{\beta}p_+^2 \\ p_- & \bar{\beta}p_-^2 & \bar{M}_2^- \end{pmatrix} \quad (\text{S4})$$

$$\Lambda = \begin{pmatrix} 0 & 0 & \bar{\lambda}_3 \\ 0 & 0 & 0 \\ \bar{\lambda}_3 & 0 & 0 \end{pmatrix}, \quad \Delta = \begin{pmatrix} \Delta_1(r)e^{i\theta} & 0 & 0 \\ 0 & \Delta_2^+(r)e^{i\theta} & 0 \\ 0 & 0 & \Delta_2^-(r)e^{i\theta} \end{pmatrix}. \quad (\text{S5})$$

The Zeeman field adds $\delta\mathcal{H} = E_Z \text{diag}(\mathbf{1}, \mathbf{1}, -\mathbf{1}, -\mathbf{1})$ to Eq. (S3) ($E_Z = g\mu_B B/2$).

The emergent rotational invariance of the $\mathbf{k} \cdot \mathbf{p}$ Hamiltonian allows to expand the wave functions at a given k_z in angular momenta l

$$\Psi_\sigma(x, y) = \sum_l U_\sigma^{(l)} \Psi_\sigma^{(l)}(r) \quad (\text{S6})$$

with

$$U_\uparrow^{(l)} = \text{diag}(e^{il\theta - i\pi/4}, e^{i(l-1)\theta + i\pi/4}, e^{i(l+1)\theta + i\pi/4}, e^{i(l-1)\theta - i\pi/4}, e^{i(l-2)\theta + i\pi/4}, e^{il\theta + i\pi/4}), \quad (\text{S7})$$

$$U_\downarrow^{(l)} = \text{diag}(e^{i(l+1)\theta + i\pi/4}, e^{i(l+2)\theta - i\pi/4}, e^{il\theta - i\pi/4}, e^{il\theta + i\pi/4}, e^{i(l+1)\theta - i\pi/4}, e^{i(l-1)\theta - i\pi/4}). \quad (\text{S8})$$

The relative factors of $e^{i\theta}$ in various matrix elements reflect that different orbitals transform differently under rotations. The choice of phases of $\pi/4$ is pure convenience.

Using this transformation we obtain in the l th sector

$$\mathcal{H}^{(l)} = \left(\begin{array}{cc|cc} H_\uparrow^{(l)} & \bar{\Delta} & \Lambda & 0 \\ \bar{\Delta} & -H_\uparrow^{(l-1)} & 0 & -\Lambda \\ \hline \Lambda & 0 & H_\downarrow^{(l+1)} & \bar{\Delta} \\ 0 & -\Lambda & \bar{\Delta} & -H_\downarrow^{(l)} \end{array} \right), \quad (\text{S9a})$$

with $\bar{\Delta} = \text{diag}(\Delta_1, \Delta_2^+, \Delta_2^-)$ and

$$H_\uparrow^{(l)} = \begin{pmatrix} \bar{M}_1^{(l)} & D_r^{1-l} & -D_r^{1+l} \\ -D_r^l & \bar{M}_2^{(l-1),+} & -\bar{\beta}D_r^l D_r^{l+1} \\ D_r^{-l} & -\bar{\beta}D_r^{-l} D_r^{1-l} & \bar{M}_2^{(l+1),-} \end{pmatrix}, \quad H_\downarrow^{(l)} = \begin{pmatrix} \bar{M}_1^{(l)} & D_r^{1+l} & -D_r^{1-l} \\ -D_r^{-l} & \bar{M}_2^{(l+1),+} & -\bar{\beta}D_r^{-l} D_r^{1-l} \\ D_r^l & -\bar{\beta}D_r^l D_r^{l+1} & \bar{M}_2^{(l-1),-} \end{pmatrix}. \quad (\text{S9b})$$

We introduced $D_r^k = \partial_r + k/r$ and $\bar{M}_i^k = \bar{M}_i|_{M_i^{(1)}=0} - M_i^{(1)}[D_r^{1-k}D_r^k + D_r^{1+k}D_r^{-k}]/[2\chi^2]$. The shift by $l = 1$ between particle and hole sectors is a consequence of the chosen vortex with winding $+1$. We remind ourselves that in the inner product in cylindrical coordinates is $\langle \Psi | \Phi \rangle = 2\pi \sum_l \int dr r \Psi_l^*(r) \Phi_l(r)$. This is the reason why Eq. (S9) appears non-Hermitian (it is self-adjoint but with respect to the above inner product).

To make further progress we now concentrate on the two most interesting situations when the chemical potential is near the Dirac point or near the topological anticrossing.

Case 1: Fermi energy near topological anticrossing

We begin the discussion by concentrating on the regime where the chemical potential is in the vicinity of the topological anticrossing. To find a perturbative solution, we first concentrate on Eq. (S9) near $\bar{M}_1|_{M_1^{(1)}=0}(k_z) = \bar{M}_2^-|_{M_2^{(1)}=0}(k_z)$ in the approximation of linearized momenta $\beta = M_1^{(1)} = M_2^{(1)} = 0$, setting $\bar{\lambda}_3 = 0$ and projected onto the relevant bands, i.e. $(|z, \uparrow\rangle, |(x - iy)z, \uparrow\rangle, |z, \downarrow\rangle, |(x + iy)z, \downarrow\rangle)$. We furthermore introduce ‘‘center of mass’’ $\Delta(r) = \frac{\Delta_1(r) + \Delta_2^-(r)}{2}$ and relative pairing gaps $\delta\Delta(r) = \Delta_1(r) - \Delta_2^-(r)$. The zeroth order Hamiltonian is a direct sum of \uparrow and \downarrow sectors

$$\mathcal{H}_{\uparrow,0}^{(l)} = \begin{pmatrix} -\mu_{\text{eff}} & 0 & -D_r^{1+l} & \Delta(r) & 0 & 0 \\ 0 & 0 & 0 & 0 & 0 & 0 \\ D_r^{-l} & 0 & -\mu_{\text{eff}} & 0 & 0 & \Delta(r) \\ \Delta(r) & 0 & 0 & \mu_{\text{eff}} & 0 & D_r^l \\ 0 & 0 & 0 & 0 & 0 & 0 \\ 0 & 0 & \Delta(r) & -D_r^{1-l} & 0 & \mu_{\text{eff}} \end{pmatrix}, \quad \mathcal{H}_{\downarrow,0}^{(l)} = \begin{pmatrix} -\mu_{\text{eff}} & 0 & -D_r^l & \Delta(r) & 0 & 0 \\ 0 & 0 & 0 & 0 & 0 & 0 \\ D_r^{1+l} & 0 & -\mu_{\text{eff}} & 0 & 0 & \Delta(r) \\ \Delta(r) & 0 & 0 & \mu_{\text{eff}} & 0 & D_r^{1-l} \\ 0 & 0 & 0 & 0 & 0 & 0 \\ 0 & 0 & \Delta(r) & -D_r^l & 0 & \mu_{\text{eff}} \end{pmatrix}, \quad (\text{S10})$$

Here, $\mu_{\text{eff}} = \mu - \frac{\bar{M}_1|_{M_1^{(1)}=0} + \bar{M}_2^-|_{M_2^{(1)}=0}}{2}$

We readily find that a chiral symmetry

$$\tau_y \begin{pmatrix} 0 & 0 & -i \\ 0 & 0 & 0 \\ i & 0 & 0 \end{pmatrix} \mathcal{H}_{0,\uparrow/\downarrow} \tau_y \begin{pmatrix} 0 & 0 & -i \\ 0 & 0 & 0 \\ i & 0 & 0 \end{pmatrix} = -\mathcal{H}_{0,\uparrow/\downarrow} \quad (\text{S11})$$

exists if and only if $l = 0$ in both up and down spin sectors. This chiral symmetry is the necessary ingredient for the determination of the zero energy Majorana mode in Eq. (S10). The zeroth order wave functions are thus

$$\Psi_{\uparrow}^{(l=0)}(r) = \mathcal{N} e^{-\int_0^r \Delta(r') dr'} \begin{pmatrix} J_0(\mu_{\text{eff}} r) \\ 0 \\ J_1(\mu_{\text{eff}} r) \\ J_1(\mu_{\text{eff}} r) \\ 0 \\ -J_0(\mu_{\text{eff}} r) \end{pmatrix}, \quad \Psi_{\downarrow}^{(l=0)}(r) = \mathcal{N} e^{-\int_0^r \Delta(r') dr'} \begin{pmatrix} J_1(\mu_{\text{eff}} r) \\ 0 \\ -J_0(\mu_{\text{eff}} r) \\ -J_0(\mu_{\text{eff}} r) \\ 0 \\ -J_1(\mu_{\text{eff}} r) \end{pmatrix} \quad (\text{S12})$$

Case 2: Fermi energy near the Dirac point

We now switch to the regime where the chemical potential is in the vicinity of the topological Dirac semimetal. To find a perturbative solution, we now concentrate on Eq. (S9) near $\bar{M}_1|_{M_1^{(1)}=0}(k_z) = \bar{M}_2^+|_{M_2^{(1)}=0}(k_z)$, again in the approximation of linearized momenta $\beta = M_1^{(1)} = M_2^{(1)} = 0$, setting $\bar{\lambda}_3 = 0$ and projected onto the relevant bands, which in this case are $(|z, \uparrow\rangle, |(x + iy)z, \uparrow\rangle, |z, \downarrow\rangle, |(x - iy)z, \downarrow\rangle)$. With the slightly different notations as in the previous section $\Delta(r) = \frac{\Delta_1(r) + \Delta_2^+(r)}{2}$, $\delta\Delta(r) = \Delta_1(r) - \Delta_2^+(r)$, $\mu_{\text{eff}} = \mu - \frac{\bar{M}_1|_{M_1^{(1)}=0} + \bar{M}_2^+|_{M_2^{(1)}=0}}{2}$, the zeroth order Hamiltonian is

again a direct sum of \uparrow and \downarrow sectors

$$\mathcal{H}_{\uparrow,0}^{(l)} = \begin{pmatrix} -\mu_{\text{eff}} & D_r^{1-l} & 0 & \Delta(r) & 0 & 0 \\ -D_r^l & -\mu_{\text{eff}} & 0 & 0 & \Delta(r) & 0 \\ 0 & 0 & 0 & 0 & 0 & 0 \\ \Delta(r) & 0 & 0 & \mu_{\text{eff}} & -D_r^{2-l} & 0 \\ 0 & \Delta(r) & 0 & D_r^{l-1} & \mu_{\text{eff}} & 0 \\ 0 & 0 & 0 & 0 & 0 & 0 \end{pmatrix}, \quad \mathcal{H}_{\downarrow,0}^{(l)} = \begin{pmatrix} -\mu_{\text{eff}} & D_r^{l+2} & 0 & \Delta(r) & 0 & 0 \\ -D_r^{-l-1} & -\mu_{\text{eff}} & 0 & 0 & \Delta(r) & 0 \\ 0 & 0 & 0 & 0 & 0 & 0 \\ \Delta(r) & 0 & 0 & \mu_{\text{eff}} & -D_r^{1+l} & 0 \\ 0 & \Delta(r) & 0 & D_r^{-l} & \mu_{\text{eff}} & 0 \\ 0 & 0 & 0 & 0 & 0 & 0 \end{pmatrix}, \quad (\text{S13})$$

In this energy and momentum regime, we find a chiral symmetry

$$\tau_y \begin{pmatrix} 0 & -i & 0 \\ i & 0 & 0 \\ 0 & 0 & 0 \end{pmatrix} \mathcal{H}_{0,\uparrow/\downarrow} \tau_y \begin{pmatrix} 0 & -i & 0 \\ i & 0 & 0 \\ 0 & 0 & 0 \end{pmatrix} = -\mathcal{H}_{0,\uparrow/\downarrow} \quad (\text{S14})$$

which exists if and only if $l = 1$ ($l = -1$) in the up (down) spin sectors. Keeping in mind that the chiral symmetry is necessary ingredient for the zero energy solution in Eq. (S13), the Majorana wave functions are thus in sectors of different angular momentum and therefore

$$\Psi_{\uparrow}^{(l=1)}(r) = \mathcal{N} e^{-\int_0^r \Delta(r') dr'} \begin{pmatrix} -J_1(\mu_{\text{eff}} r) \\ J_0(\mu_{\text{eff}} r) \\ 0 \\ J_0(\mu_{\text{eff}} r) \\ J_1(\mu_{\text{eff}} r) \\ 0 \end{pmatrix}, \quad \Psi_{\downarrow}^{(l=-1)}(r) = \mathcal{N} e^{-\int_0^r \Delta(r') dr'} \begin{pmatrix} J_0(\mu_{\text{eff}} r) \\ J_1(\mu_{\text{eff}} r) \\ 0 \\ J_1(\mu_{\text{eff}} r) \\ -J_0(\mu_{\text{eff}} r) \\ 0 \end{pmatrix} \quad (\text{S15})$$

We have also explicitly checked that the chiral symmetry is present (absent) in the case of a vortex with generic odd (even) winding number. The absent chiral symmetry for even winding prevents helical Majorana modes.

Approximate dispersion relations

We now use the previously derived low-energy solutions to determine the effective Hamiltonian of Majorana vortex states. We use $\Delta_i(r) = \Delta_i^\infty \tanh(r/\xi)$ and $(\Delta_1^\infty + \Delta_2^\infty)\xi \equiv 2\Delta^\infty\xi = 2$ with $i = (1, 2, 3) = (1, 2_+, 2_-)$ and $\Delta_2^+ = \Delta_2^-$ in the following - but the qualitative aspects are expected to be insensitive to this precise choice. We further define the following integrals

$$I_+(x) = \int_0^\infty dr \frac{r}{[\cosh(r/x)]^2} (J_0(r)^2 + J_1(r)^2) \simeq \frac{|x| (2 - \pi |x| \log(\cosh(\frac{2}{\pi x})))}{\pi}, \quad (\text{S16})$$

$$I_-(x) = \int_0^\infty dr \frac{r}{[\cosh(r/x)]^2} (J_0(r)^2 - J_1(r)^2) \simeq \begin{cases} x^2 \ln(2), & x \ll 1 \\ \frac{1}{4x}, & x \gg 1, \end{cases} \quad (\text{S17})$$

$$I_0(x) = \int_0^\infty dr \frac{r \sinh(r/x)}{[\cosh(r/x)]^3} 2J_0(r)J_1(r) = x I_-(x). \quad (\text{S18})$$

The expectation value of the full Hamiltonian with respect to the wave function of Majorana solution leads to the first perturbative low energy Hamiltonian (we here present only the case of linearized dispersion). For case 1, in the basis $\{\Psi_{\uparrow}^{(l=0)}, \Psi_{\downarrow}^{(l=0)}\}$ we obtain

$$\mathcal{H} \simeq \begin{pmatrix} (M_1 - M_2^-) \frac{I_-(\frac{\mu_{\text{eff}}}{\Delta_{\infty}^{\text{eff}}})}{2I_+(\frac{\mu_{\text{eff}}}{\Delta_{\infty}^{\text{eff}}})} + (\Delta_1^\infty - \Delta_2^\infty) \frac{I_0(\frac{\mu_{\text{eff}}}{\Delta_{\infty}^{\text{eff}}})}{2I_+(\frac{\mu_{\text{eff}}}{\Delta_{\infty}^{\text{eff}}})} + E_Z & -\bar{\lambda}_3 \frac{I_-(\frac{\mu_{\text{eff}}}{\Delta_{\infty}^{\text{eff}}})}{I_+(\frac{\mu_{\text{eff}}}{\Delta_{\infty}^{\text{eff}}})} \\ -\bar{\lambda}_3 \frac{I_-(\frac{\mu_{\text{eff}}}{\Delta_{\infty}^{\text{eff}}})}{I_+(\frac{\mu_{\text{eff}}}{\Delta_{\infty}^{\text{eff}}})} & -(M_1 - M_2^-) \frac{I_-(\frac{\mu_{\text{eff}}}{\Delta_{\infty}^{\text{eff}}})}{2I_+(\frac{\mu_{\text{eff}}}{\Delta_{\infty}^{\text{eff}}})} - (\Delta_1^\infty - \Delta_2^\infty) \frac{I_0(\frac{\mu_{\text{eff}}}{\Delta_{\infty}^{\text{eff}}})}{2I_+(\frac{\mu_{\text{eff}}}{\Delta_{\infty}^{\text{eff}}})} - E_Z \end{pmatrix}. \quad (\text{S19})$$

In contrast, for case 2, i.e. a Fermi energy near the Dirac crossing, we find in the basis of $\{\Psi_{\uparrow}^{(l=+1)}, \Psi_{\downarrow}^{(l=-1)}\}$

$$\mathcal{H} \simeq \begin{pmatrix} -(M_1 - M_2^+) \frac{I_-(\frac{\mu_{\text{eff}}}{\Delta^\infty})}{2I_+(\frac{\mu_{\text{eff}}}{\Delta^\infty})} - (\Delta_1^\infty - \Delta_2^\infty) \frac{I_0(\frac{\mu_{\text{eff}}}{\Delta^\infty})}{2I_+(\frac{\mu_{\text{eff}}}{\Delta^\infty})} + E_Z & 0 \\ 0 & (M_1 - M_2^+) \frac{I_-(\frac{\mu_{\text{eff}}}{\Delta^\infty})}{2I_+(\frac{\mu_{\text{eff}}}{\Delta^\infty})} + (\Delta_1^\infty - \Delta_2^\infty) \frac{I_0(\frac{\mu_{\text{eff}}}{\Delta^\infty})}{2I_+(\frac{\mu_{\text{eff}}}{\Delta^\infty})} - E_Z \end{pmatrix}. \quad (\text{S20})$$

We thus observe that near the topological anticrossing, Majorana modes of $l = 0$ mutually gap out, Fig. 1 b) of the main text, while at the Dirac point, C_4 symmetry protects the appearance of helical Majorana modes Fig. 1 d) of the main text. This section also concludes the derivation of the velocity $v_M^{| \mu_{\text{eff}} | \gg \Delta^\infty} (\Delta^\infty / \mu_{\text{eff}})^2 \partial_{k_z} |_{k_z^*} [M_1 - M_2^+]$ of the helical Majorana modes. An analogous result with the same factor $(\Delta^\infty / \mu_{\text{eff}})^2$ and obtained by different means for the case of a the o-vortex in $^3\text{He-B}$ was presented in Eq. (7.2) of Ref. [18]. We also highlight that in the limit $|\mu_{\text{eff}}| \ll \Delta^\infty$ the velocity is $v_M \simeq \partial_{k_z} |_{k_z^*} [M_1 - M_2^+]/2$.

INDEX THEOREM

In this section we summarize the semiclassical evaluation of the index Eq. (3) of the main text which ensures the appearance of propagating Majorana fermions. The definition and the idea of a semiclassical evaluation of the index follows Ref. [36] for superfluid ^3He . However the connection to the Berry curvature monopoles was not drawn in that context.

In contrast to all other parts of this work, z here denotes the direction of the vortex line and is in general not the same as the (001) direction of the crystal.

Non-degenerate Fermi surface - semiclassical expansion

Let's consider a Bogoliubov-de Gennes Hamiltonian of each non-degenerate system separately

$$\mathcal{H}_\pm = \hat{\mathbf{d}}_\pm \cdot \boldsymbol{\tau}. \quad (\text{S21})$$

with $\hat{\mathbf{d}}$ a three vector of which each component is an operator in real/momentum space and $\boldsymbol{\tau}$ representing Pauli matrices in Nambu space. As we readily show, such a Hamiltonian may be obtained by projecting Eq. (1) or any other Hamiltonian with non-degenerate bands onto the conduction band.

Using $[i\epsilon - \hat{\mathbf{d}} \cdot \boldsymbol{\tau}]^{-1} = (i\epsilon + \hat{\mathbf{d}} \cdot \boldsymbol{\tau})[\epsilon^2 + \hat{v}d^2 + \frac{i}{2}\epsilon_{abc}[\hat{d}_a, \hat{d}_b]\tau_c]^{-1} = [\epsilon^2 + \hat{v}d^2 + \frac{i}{2}\epsilon_{abc}[\hat{d}_a, \hat{d}_b]\tau_c]^{-1}(i\epsilon + \hat{\mathbf{d}} \cdot \boldsymbol{\tau})$ and expanding to leading order in the commutator leads to

$$N(k_z) = -\frac{i}{2} \sum_{\pm} (\pm 1) \int \frac{d\epsilon}{2\pi} \epsilon_{abc} \sum_{\mathbf{p}} \{ \hat{d}_{c,\pm} \circ [\epsilon^2 + \hat{\mathbf{d}}_\pm^2]^{-1} \circ [\hat{d}_{a,\pm} \circ \hat{d}_{b,\pm}] \circ [\epsilon^2 + \hat{\mathbf{d}}_\pm^2]^{-1} \}_{\mathbf{p},\mathbf{p}} \quad (\text{S22})$$

Here, momentum space has been used to visualize the meaning of the trace operation.

Standard Moyal product and a simplified case

We make use of the concepts of Wigner transformation and Moyal product, see e.g. A. Kamenev, *Field Theory of Non-Equilibrium Systems*, Cambridge University Press (2011). For arbitrary operators \hat{A}, \hat{B} this implies

$$A(\mathbf{X}, \mathbf{P}) = \int \frac{d^2 \Delta \mathbf{p}}{(2\pi)^2} A(\mathbf{P} + \frac{\Delta \mathbf{p}}{2}, \mathbf{P} - \frac{\Delta \mathbf{p}}{2}) e^{i\Delta \mathbf{p} \cdot \mathbf{X}}, \quad (\text{S23})$$

$$[A \circ B](\mathbf{X}, \mathbf{P}) = A(\mathbf{X}, \mathbf{P}) e^{\frac{i}{2} (\overleftarrow{\nabla}_X \overrightarrow{\nabla}_P - \overleftarrow{\nabla}_P \overrightarrow{\nabla}_X)} B(\mathbf{X}, \mathbf{P}), \quad (\text{S24})$$

where \circ denotes subsequent application of operators. Derivatives in real and momentum space ∇_X and ∇_P acting to the left (right) are denoted by arrows \leftarrow (\rightarrow) in the superscript. Leading order expansion in gradients leads to

$$N(k_z) = \frac{1}{2} \sum_{\pm} (\pm 1) \int \frac{d^2 P d^2 X}{(2\pi)^2} \epsilon_{abc} \frac{d_{a,\pm}(\mathbf{X}, \mathbf{P})}{d_{\pm}(\mathbf{X}, \mathbf{P})} \overleftarrow{\nabla}_X \frac{d_{b,\pm}(\mathbf{X}, \mathbf{P})}{d_{\pm}(\mathbf{X}, \mathbf{P})} \cdot \overrightarrow{\nabla}_P \frac{d_{c,\pm}(\mathbf{X}, \mathbf{P})}{d_{\pm}(\mathbf{X}, \mathbf{P})}. \quad (\text{S25})$$

We first consider the simplified case where we linearize a generic elliptical vortex in an orbital independent order parameter field. We consider a Hamiltonian of the form

$$\mathcal{H} = \begin{pmatrix} H_{\mathbf{p}} - \mu & \Delta_{\infty} \left(\frac{x}{\xi_x} - i \frac{y}{\xi_y} \right) \\ \Delta_{\infty} \left(\frac{x}{\xi_x} + i \frac{y}{\xi_y} \right) & \mu - H_{\mathbf{p}} \end{pmatrix} \quad (\text{S26})$$

Projected onto the conduction band $H_{\mathbf{p}} |u_{\mathbf{p}}\rangle = \epsilon_{\mathbf{p}} |u_{\mathbf{p}}\rangle$, $\mathcal{H} = \hat{\mathbf{d}} \cdot \boldsymbol{\tau}$ with

$$\hat{\mathbf{d}} = (\Delta_{\infty} [i\partial_x + \mathcal{A}_x] / \xi_x, \Delta_{\infty} [i\partial_y + \mathcal{A}_y] / \xi_y, \epsilon_{\mathbf{p}} - \mu). \quad (\text{S27})$$

and $i\mathcal{A}_{x,y} = i\langle u_{\mathbf{p}} | \partial_{p_{x,y}} | u_{\mathbf{p}} \rangle$ denotes the Berry connection. With the above mentioned Wigner transform we obtain $\mathbf{d}(\mathbf{X}, \mathbf{P}) = (\Delta_{\infty}(X + \mathcal{A}_x) / \xi_x, \Delta_{\infty}(Y + \mathcal{A}_y) / \xi_y, \epsilon_{\mathbf{p}} - \mu)$. We use that the contribution of $c = z$ to Eq. (S25)

$$\int \frac{d^2 P d^2 X}{(2\pi)^2} \epsilon_{abz} \frac{d_a(\mathbf{X}, \mathbf{P})}{d(\mathbf{X}, \mathbf{P})} \nabla_X \frac{d_b(\mathbf{X}, \mathbf{P})}{d(\mathbf{X}, \mathbf{P})} \cdot \nabla_P \frac{d_z(\mathbf{X}, \mathbf{P})}{d(\mathbf{X}, \mathbf{P})} = \int \frac{d^2 P d^2 X}{(2\pi)^2} \epsilon_{abz} \frac{d_a(\mathbf{X}, \mathbf{P})}{d(\mathbf{X}, \mathbf{P})^3} v_b(\mathbf{P}) \frac{\Delta_{\infty}}{\xi_b} = 0 \quad (\text{S28})$$

where at the last equality sign we took the \mathbf{X} integral first and shifted $X_a \rightarrow (\mathbf{X} - \mathbf{A})_a / \xi_a$.

Then, we obtain

$$N(k_z) = \sum_{\pm} (\pm 1) \frac{\Delta_{\infty}^2}{2\xi_x \xi_y} \int \frac{d^2 P d^2 X}{(2\pi)^2} \frac{d_3(\mathbf{X}, \mathbf{P})}{d^3(\mathbf{X}, \mathbf{P})} \Omega_z^{\pm}. \quad (\text{S29})$$

Gauge invariant Wigner transform and generic case

For a more generic coordinate dependence of the order parameter it is advantageous to define a Wigner transform which respects the gauge invariance $|u_{\mathbf{p}}\rangle \sim e^{i\phi_{\mathbf{p}}} |u_{\mathbf{p}}\rangle$ of eigenstates. Starting from the projection $A(\mathbf{p}, \mathbf{p}') = \langle u_{\mathbf{p}} | \hat{A}(\mathbf{p}, \mathbf{p}') | u_{\mathbf{p}'} \rangle$ of an orbital matrix $\hat{A}(\mathbf{p}, \mathbf{p}')$ onto a single, given band at the Fermi surface we define

$$A(\mathbf{X}, \mathbf{P}) = \int \frac{d\Delta \mathbf{p}}{(2\pi)^2} A(\mathbf{P} + \Delta \mathbf{p}/2, \mathbf{P} - \Delta \mathbf{p}/2) e^{i\Delta \mathbf{p} \cdot (\mathbf{X} - \mathbf{A}(\mathbf{P}))}. \quad (\text{S30})$$

This Wigner transform is gauge invariant to zeroth and first order in gradient expansion and the momentum space analogue of the Wigner transform in the presence of a magnetic field, see B.L. Al'tshuler, JETP **48**, 670 (1978). As a consequence, the Moyal product takes the form

$$[A \circ B](\mathbf{X}, \mathbf{P}) \simeq A(\mathbf{X}, \mathbf{P}) B(\mathbf{X}, \mathbf{P}) + \frac{i}{2} (\vec{\nabla}_X A \cdot \vec{\nabla}_P B - \vec{\nabla}_P A \cdot \vec{\nabla}_X B) + \frac{i}{2} \vec{\Omega} \cdot (\vec{\nabla}_X A \times \vec{\nabla}_X B). \quad (\text{S31})$$

Since we here concentrate for a 2D problem for each k_z separately, in the anomalous last term only Ω_z enters. Using this definition of the Wigner transform we have

$$\mathbf{d}(\mathbf{X}, \mathbf{P}) = (\text{Re}\Delta(\mathbf{X}, \mathbf{P}), -\text{Im}\Delta(\mathbf{X}, \mathbf{P}), \epsilon_{\mathbf{P}} - \mu) \quad (\text{S32})$$

with $\Delta(\mathbf{X}, \mathbf{P})$ the semiclassical gap function in the band under consideration. Then we find for $N(k_z) = N_{\mathcal{H}_+}(k_z) - N_{\mathcal{H}_-}(k_z)$

$$N_{\mathcal{H}_{\pm}}(k_z) = \frac{1}{4} \int \frac{d^2 P d^2 X}{(2\pi)^2} \epsilon_{abc} \{ 2\hat{d}_a \vec{\nabla}_X \hat{d}_b \cdot \vec{\nabla}_P \hat{d}_c + \hat{d}_a (\vec{\nabla}_X \hat{d}_b \times \vec{\nabla}_X \hat{d}_c) \cdot \vec{\Omega}^{\pm} \}. \quad (\text{S33})$$

(In general $\hat{\mathbf{d}} = \mathbf{d}/d$ may also differ between $+/-$ sectors.) Straightforward inspection of this equation for the simplified model Eq. (S26) reproduces Eq. (S29).

For a generic vortex in the context of FeSCs we find

$$\mathbf{d}(\mathbf{X}, \mathbf{P}) = \left(\frac{X}{R} d_{\perp}(\mathbf{P}, R), \frac{Y}{R} d_{\perp}(\mathbf{P}, R), d_3(\mathbf{P}) \right) \quad (\text{S34})$$

independently of \pm . For the simplest case of a two band model $H(\mathbf{k}) = \sum_{\mu=0}^3 h_{\mu}(\mathbf{k}) \sigma_{\mu}$ with a gap function $\Delta_0 \mathbf{1} + \Delta_3 \sigma_z$ and a standard $\tanh(r/\xi)$ vortex we obtain (here $\xi = \pm 1$ stands for conduction/valence band)

$$d_{\perp}(\mathbf{P}, R) = [\Delta_0 + \xi \Delta_3 h_3(\mathbf{P}) / |\mathbf{h}(\mathbf{P})|] \tanh(R/\xi); d_3(\mathbf{P}) = h_0(\mathbf{P}) + \xi |\mathbf{h}(\mathbf{P})| - \mu. \quad (\text{S35})$$

We introduce

$$\tilde{n}(\mathbf{X}, \mathbf{P}) = \int \frac{d\epsilon}{2\pi} \frac{d_3(\mathbf{P})}{\epsilon^2 + d^2(\mathbf{X}, \mathbf{P})} = - \int \frac{d\epsilon}{4\pi} \text{tr} [\mathcal{G}(\epsilon; \mathbf{X}, \mathbf{P}) \tau_z] = \frac{d_3(\mathbf{P})}{2d(\mathbf{X}, \mathbf{P})} \quad (\text{S36})$$

With this expression we can write $N_{\mathcal{H}_\pm}(k_z) = N_{\mathcal{H}_\pm}(k_z)|_1 + N_{\mathcal{H}_\pm}(k_z)|_2$ with

$$\begin{aligned} N_{\mathcal{H}_\pm}(k_z)|_1 &= \frac{1}{2} \int \frac{d^2 P d^2 X}{(2\pi)^2} \epsilon_{abc} \hat{d}_a \vec{\nabla}_X \hat{d}_b \cdot \vec{\nabla}_P d_c \\ &= \frac{1}{2} \int \frac{d^2 P d^2 X}{(2\pi)^2} \frac{1}{d^3 R^2} \hat{e}_z \cdot [d_\perp^2 (\mathbf{X} \times \vec{\nabla}_P d_3) - d_\perp d_3 (\mathbf{X} \times \vec{\nabla}_P d_\perp)] \\ &= \frac{1}{2} \int \frac{d^2 P d^2 X}{(2\pi)^2} \frac{1}{R^2} \hat{e}_z \cdot (\mathbf{X} \times \vec{\nabla}_P \frac{d_3}{d}) \\ &= \int \frac{d^2 P d^2 X}{(2\pi)^2} \frac{1}{R^2} \hat{e}_z \cdot (\mathbf{X} \times \vec{\nabla}_P \tilde{n}(\mathbf{X}, \mathbf{P})). \end{aligned} \quad (\text{S37})$$

This expression vanishes from the total index if $\tilde{n}^+ = \tilde{n}^-$ (this is the case here). Furthermore

$$\begin{aligned} N_{\mathcal{H}_\pm}(k_z)|_2 &= \frac{1}{4} \int \frac{d^2 P d^2 X}{(2\pi)^2} \epsilon_{abc} \hat{d}_a (\vec{\nabla}_X \hat{d}_b \times \vec{\nabla}_X \hat{d}_c) \cdot \vec{\Omega}^\pm \\ &= -\pi \int \frac{d^2 P d^2 X}{(2\pi)^2} \frac{\Omega_z^\pm}{R} \partial_R \frac{d_3}{d} \\ &= -2\pi \int \frac{d^2 P}{(2\pi)^2} \Omega_z^\pm \int_0^\infty d\mathbf{R} \cdot \vec{\nabla}_R \tilde{n}(\mathbf{X}, \mathbf{P}) \end{aligned} \quad (\text{S38})$$

We thus obtain the final result

$$N(k_z) = N_{\mathcal{H}_+}(k_z) - N_{\mathcal{H}_-}(k_z) = 2\pi \int \frac{d^2 P}{(2\pi)^2} [\Omega_z^-(\mathbf{P}) - \Omega_z^+(\mathbf{P})] \int_0^\infty d\mathbf{R} \cdot \vec{\nabla}_R \tilde{n}(\mathbf{X}, \mathbf{P}) \quad (\text{S39})$$

We emphasize that, in the regime of applicability of semiclassics, this expression is generic and not restricted to FeSC, only. It is also possible to incorporate generic winding by

$$\mathbf{d}(\mathbf{X}, \mathbf{P}) = \left(\text{Re} \left[\frac{(X + iY)^{\nu_v}}{R^{\nu_v}} \right] d_\perp(\mathbf{P}, R), \text{Im} \left[\frac{(X + iY)^{\nu_v}}{R^{\nu_v}} \right] d_\perp(\mathbf{P}, R), d_3(\mathbf{P}) \right). \quad (\text{S40})$$

Using

$$\vec{\nabla}_X d_x \times \vec{\nabla}_X d_y = \frac{\nu_v}{2R} \partial_R d_\perp \hat{e}_z, \quad (\text{S41})$$

we readily find that the index (S39) acquires a multiplication of ν_v . This concludes the derivation of Eq. (4) of the main text.
